The Self-Acting, Subambient Foil Bearing in High Speed, Contact Tape Recording with a Flat Head

Sinan Müftü and Hans F. Hinteregger

Massachusetts Institute of Technology

Haystack Observatory

Westford, Massachusetts 01886

ABSTRACT

The mechanics and tribology of a flat head for high-speed, contact tape recording is presented. Experiments performed on a "row-bar" of thin-film disk-heads where the tape is wrapped only on the edge opposite to the heads showed very stable contact for a wide range of tape speeds and very low wear. A model of the interface showed that a self-acting, subambient air-bearing forms near the leading wrapped corner. This suction is caused by the expansion of air into the diverging gap on the upstream side of the head-tape interface, which is unique to this wrap geometry, and it is responsible for the stability and low contact pressures. A bidirectional version of a flat head geometry is analyzed via modeling and suggestions are made for that design. This work also showed strong evidence of a treshold of contact pressure below which wear becomes negligable.

1

INTRODUCTION

Increasing demands on data storage rates and capacities require modern tape drives to record in full contact with the tape at high speeds. In this operation regime, the overall head-wear and recession at the magnetic poles can become a problem. Using wear resistant head materials and surface overcoats improves the head's wear life (1,2). In general, the wear rate is inversely proportional to the hardness of the material (3,4). Micro- and nano-wear measurement experiments show that very small wear volumes will result under very low contact pressures (5). Therefore, the design of a contact-recording-tape-head should involve a hard load bearing surface, and it should ensure low enough contact pressures while preventing the tape to separate from the head due to self-air-lubrication.

The flat thin-film head that we evaluated for tape recording proved to be a promising candidate for realizing these requirements. In an experiment, a "row-bar" of thin-film disk-heads were evaluated for tape recording by wrapping the tape as shown in Figure 1 (6). In this wrap geometry the tape is in contact with the head only when it runs from left-to-right as shown in this figure. The main three results important for tribology and recording were: a) no detectable head wear at the end of more than 2000 hours of the shuttling, b) constancy of head-tape spacing in 0.5-8 m/s tape speed range, and c) maintability of performance for the entire duration of the experiment (6,7).

An explanation of the experimental results was obtained by modeling the head-tape interface. In this model the steady state equilibrium of the tape displacements was obtained including the air lubrication effects and compliance of the tape asperities. The wear of the head was also included in the model. Similar studies of the head-tape interface have been reported in (8-11).

This model showed that the air entrained in the interface, due to self-lubrication, expands in

the bump near the wrapped corner. This causes the air pressure to become subambient and explains the good performance at high tape speeds. Conventional tape recording heads have circular cross-sections with longitudinally or laterally oriented pressure-relief slots to maintain head-tape contact especially at high tape speeds. In contrast, the flat-head concept is considerably simpler in terms of manufacturing, and it seems to show good speed-independent performance and low wear. Explanation of the mechanics of the flat-head from a tribological point of view, is the subject of this paper.

EXPERIMENTAL RESULTS

We used a row-bar of thin-film disk-heads to evaluate their read-performance for high speed, and high density, contact tape recording using two different video tapes. The read-elements on these disk-heads were 3.75 μm wide, 2 μm deep magnetoresistive (MR) heads. These heads were deposited on a hard Al_2O_3-TiC (Altic) substrate. The deposited layers are sputtered Al_2O_3 (alumina) as undercoat, gap-spacer and overcoat, $Ni_{0.2}Fe_{0.8}$ (Permalloy) as shield and pole-pieces and MR element layers. The thickness of the thin-film layer is ~ 30 μm. Altic surface constitutes most of the load bearing surface shown in Figure 1.

The tapes used in the evaluation were 2.54 cm wide SVHS-like (Sony DK15500) and 1.27 cm wide WVHS-like (Fuji) tapes. The WVHS was a double coated metal particle (MP) tape and the SVHS was a Co-γ-Fe_2O_3 tape. The SVHS and WVHS tapes were shuttled end-to-end for 2,000 hours and 120 hours in the contact direction at 8 m/s, respectively. The experiments were carried out on a Metrum 96 tape drive and the 86.96 N/m of tape tension was supplied by vacuum columns. We did not change the tapes for two reasons; a) the primary goal of the experiment was

to investigate narrow track playback characteristics of the thin-film MR heads, and b) in the Very Long Baseline Interferometry operations, for which we set our goals, virgin tapes are seldom used (12). In addition to this it should be mentioned that Bhushan and Lowry found that the initial and long term abrasivity of the virgin samples of these tapes is very low due to their exceptionally smooth surface (3).

We found that in the contact direction the head-tape spacing over the read gap remains essentially constant in the 0.5-8 m/s speed range under 86.96 N/m tension. We also detected less than 8 nm of wear of the read element after 2000 hours of shuttling in contact. The details are reported by Hinteregger and Müftü (6).

The row-bar used was 5.08 cm long. We ran the tape only on one side of this row-bar and let the other side untouched. At the end of the experiments the surface of the row-bar was probed with a stylus profilometer (Dektak-8000 with 2.5 μm radius tip). The surface on which the tape was run was compared against the virgin surface.

The surface profile measurements were made on five different locations on each worn edge and the results were averaged. Typical surface profile traces for the leading and trailing edges are given in Figure 2. The surface profiles on the virgin surface do not have the wear shown on this figure. The leading edge was worn to a 33 μm wide, 238 nm deep "bevel". The trailing edge also showed some wear, but this was less than the leading edge. Here, the average width and depth of wear were 29 μm and 83 nm, respectively.

THE HEAD-TAPE INTERFACE MODEL

The tape displacement is modeled with the equation of equilibrium of a moving beam (13). In

4

this paper we neglect the width wise variations. At steady state the equation of equilibrium for a moving beam is

$$D\frac{d^4w}{dx^4} + (\rho_a V_x^2 - T_x)\frac{d^2w}{dx^2} = p_{net} + P_c \qquad [1]$$

where the out-of-plane tape displacement is w, bending stiffness of the tape is $D = Ec^3/12(1-\nu^2)$, the tape tension is T_x, the tape transport speed is V_x, the gage pressure is $p_{net} = p - P_a$, the ambient air pressure is P_a, the contact pressure is P_c. the modulus of elasticity is E, Poisson's ratio is ν, and tape thickness is c, the coordinate axis along the undeflected tape is x, and the mass density of the tape per unit area is ρ_a.

The air lubrication effects are modeled by using the Reynolds equation including the air compressibility and first order slip flow corrections (14). Assuming that air flow is only in the running direction of the tape this equation reduces to the following form;

$$\frac{d}{dx}[ph^3\frac{dp}{dx}(1 + 6\frac{\lambda_a}{h})] = 6\mu V_x\frac{d(ph)}{dx} \qquad [2]$$

where air pressure is p, head-tape spacing is h, air viscosity is μ, and length of the molecular mean free path for air is λ_a.

In a numerical solution the contact pressure can be applied to the tape's equilibrium equation in the following way (15);

$$P_c = f(h)H(-(h - \sigma_T)) \qquad [3]$$

where H is the Heaviside step function, and σ_T is a treshold value for the separation of the contacting surfaces above which contact pressure is not applied. For $f(h)$ we used the empirically determined asperity compliance function

$$P_c = \frac{P_o}{\sigma_t^2}(h - \sigma_t)^2 \qquad [4]$$

where P_o is a constant obtained by extrapolating the experimentally determined, parabolic compli-

ance curve to $h = 0$ (8,11).

The head-tape spacing is calculated by adding the tape displacement to the mathematical description of the head shape $\delta(x)^{I_w}$;

$$h = w + \delta^{I_w} \tag{5}$$

The head shape is subject to change due to wear. In this work and others (9,16) head wear is calculated incrementally, using Archard's wear law. In the above equation the superscript I_w indicates the wear iteration level. Using Archard's wear law the depth of wear, $\delta_w^{I_w}$, after each wear iteration is calculated by,

$$\delta_w^{I_w} = k \frac{L}{H^*} P_c \tag{6}$$

where, k is an experimentally determined wear coefficient, L is the length of the tape sliding on the head, H^* is the hardness of the head material and P_c is the apparent contact pressure as described above. The head shape after each wear iteration is calculated as;

$$\delta(x)^{I_w+1} = \delta(x)^{I_w} + \delta_w(x)^{I_w}. \tag{7}$$

In general, the wear coefficient is determined experimentally. Bhushan and Lowry reported that the wear rate of Altic against CrO_2 magnetic tape is 1.1 nm/km (3). Using the parameters reported in their paper the wear coefficient, k, is calculated from this value to be 190×10^{-9} ($H = 18.2$ GPa, and $P_c = 105$ kPa).

There is experimental evidence to indicate that CrO_2 tape is more abrasive than the two tapes used in our experiments (3,16). Therefore, we feel that the wear coefficient obtained by Bhushan and Lowry is a safe upper limit especially considering that they used a high contact pressure (105 kPa) in their experiment.

The Boundary Conditions

The strain free configuration of the tape is parallel to the flat surface of the head. The displacements on the left and the right side supports are indicated by U_L and U_R. For the one sided wrap $U_R = 0$. The displacements asymptotically approach zero at the flat parts of the tape. The air pressure is ambient at the corners of the head. These boundary conditions lead to the following equations;

$$
\begin{aligned}
\text{at } x = 0, \quad w &= U_L, \quad \frac{dw}{dx} = \frac{U_L}{L_{t1}} \\
\text{at } x = L, \quad w &= U_R, \quad \frac{dw}{dx} = -\frac{U_R}{L_{t2}}
\end{aligned}
$$

[8]

$$
\begin{aligned}
\text{at } x = x_{LE}, \quad p &= P_a \\
\text{at } x = x_{TE}, \quad p &= P_a
\end{aligned}
$$

The lengths L_{t1}, and L_{t2} are indicated as 3.2 mm and 14 mm in Figure 1, respectively.

The Solution Method

Equations [1-5], and [8] form a system of equations which model the equilibrium of tape, air bearing, and contact pressure at steady state. The numerical solution algorithm that we used for these nonlinear set of equations is given in (13). Superimposed on these equations is the head wear equations described by [6] and [7]. Here we added an additional wear iteration loop outside the one which solves w, p, and P_c simultaneously. The wear calculations are performed after a converged solution for w, p and P_c is found and the head shape is updated as described above.

NUMERICAL RESULTS

Evaluation of the Wear Model

The wrap geometry shown in Figure 1 was modeled with a wear constant $C = k\frac{L}{H^*} = 1 \times 10^{-15}$ m/Pa. The other parameters used in the solution are given in Table 1. The results of the program are compared on the leading edge with the measured worn profile in Figure 3. This figure shows that at 300 wear iterations the theoretically calculated wear profile matches the experimentally measured one almost perfectly. This figure also shows the contact pressure distribution calculated by the program.

The Self-Acting, Subambient Air Bearing

As we mentioned above the experiments showed that the head-tape spacing over the MR gap essentially stays on the asperity level of the tape surface over a wide range of speeds (6). This is contrary to the more familiar case of increasing spacing with tape speed when the head has a circular shape (17). Our model showed that a "self-acting, subambient air bearing" is responsible for the speed independence of the gap spacing. Use of subambient pressure is familiar to the hard disk drive applications in the "zero-pressure" sliders (18). The stability of some tape head shapes which cause diverging head-tape spacing have been reported by Brewen et al. (19). In all three of these cases expansion of air due to a diverging channel causes subambient air pressure.

Figure 4.a shows the head-tape spacing and air pressure profiles at steady state near the leading edge. Here, we see that the air pressure is subambient. This subambient region spans the entire length of the head. The contact pressure which is not shown on this figure counteracts the air pressure to satisfy the equilibrium.

The subambient pressure acts in three regions. The "entry-region" is over the worn out bevel

8

on the leading edge. In this region, air is entrained and highest contact pressures occur. When tape is wrapped around a "sharp" corner it takes the shape of a bump whose height and width depend on the bending stiffness of the tape and the applied tension. Under this bump lies the "expansion-region" where the air pressure falls to subatmospheric values. No head-tape contact occurs in this region. The third region is the "constant-spacing" region where the spacing, and the contact and air pressures remain constant. This region constitutes most of the contact region, and here the contact pressure equals the subambient air pressure.

Figure 4.b shows the Couette, $q_1 = V_x h/2$, and the Poiseuille, $q_2 = -\frac{h^2}{12\mu}\frac{dp}{dx}(h + 6\lambda_a)$, components of the total air flow, $q = q_1 + q_2$, as well as schematic representations of the air velocity distributions in the interface. Here, we see that the Poiseuille component of the flow is positive in the 0-50 μm range. This causes air to rush into the interface and thus attain a subambient pressure. However, further along the interface the Poiseuille flow becomes negative, indicating a resistance to the flow, partly due to the converging shape of the channel. We see that the pressure rises to a certain extent but still remains subambient in the rest of the interface.

The Effect of Tape Speed and Tension on the Head-Tape Spacing

The strength of the suction generated in the interface depends on the tape speed, tension, bending stiffness and wrap angle. Figure 5.a shows that the tape would stay in contact with the head ($h \leq 48$ nm) for 1-32 m/s speed range when the tape is wrapped 2.2^o on the leading edge under 86.96 N/m tension. This figure indicates that some separation is predicted at the lowest tape speed 0.5 m/s. A minimum spacing of 46 nm is reached at 3.5 m/s tape speed and spacing increases slightly at higher speeds due to higher shear.

9

Figure 5.b shows the effects of varying the tape tension for the same geometry at 8 m/s. Here we see that the tape would contact the head when tension is greater than ∼45 N/m.

The Effect of Different Wrap Angles On Suction

In order to see the effect of different initial wrap angles on the interface we simulated the wear for wrap angles between 0.5^o and 4°. The tape speed and tension were 8 m/s and 86.96 N/m, respectively, and 300 wear iterations were considered. The results are given in Figure 6. In part (a) of this figure the worn head shape and the tape displacement at the leading edge are shown for 0.5^o and 4°. Here we see that the amplitude of the bump in the expansion-region at 4° wrap is more than three times than it is at 0.5^o. Figure 6.b shows the air pressure profiles for 0.5^o, 2°, and 4° near the leading edge. Here we see that higher wrap angles create higher subambient pressures, due to the having "deeper" expansion-regions. For the wrap angles studied here the maximum suction values occur for 4° wrap. The maximum and constant-spacing region suction values are given in Table 2.

The Effect of Different Wrap Angles On Wear

The Leading Edge Wear

Figure 7 shows calculated leading and trailing edge wear profiles for $0.5^o - 4^o$ wraps for 300 wear-iterations. On the leading edge we see that the length of the wear profile is 37 μm and it is nearly independent of the wrap angle. The shape of the wear profile closely follows the shape of the tape which has an exponential form. We calculated an approximate wear angle for each one of the profiles by connecting the lowest and highest wear points in the worn zone by a straight line. We

note that these "wear angles", presented in Table 2, are considerably lower than the wrap angles. The ratio of the initial warp angle to the approximate wear angle of the bevel is seen to be $\sim 1/6$ for c = 15.2 μm, and $T_x = 86.96$ N/m.

The Trailing Edge Wear

The thin-film head region on the trailing edge is softer than Altic. This region consists of a $\sim 3\mu$m thick alumina layer sputtered on Altic, as undercoat, followed by a $\sim 10\mu$m thick Permalloy layer and a $\sim 15\mu$m thick alumina layer, as overcoat. For Altic, by using $k = 190 \times 10^{-9}$ from (3) and $H^* = 23.5$ GPa we see that each wear iteration corresponds to roughly 121 m of tape sliding against the head. As for permalloy, we were able to obtain wear coefficients, k, from published data only for similar materials. In particular, we used the wear data for plasma sprayed alumina in place of sputtered alumina and Mn-Zn-Ferrite in place of Permalloy. We, then, calculated the wear constants, C, for 121 m of sliding as shown in Table 3. The wear coefficients and hardness values of the substitute materials are expected to be within the same order of magnitude as the actual ones; k for Permalloy is lower than Mn-Zn-Ferrite (1) and hardness of sputtered alumina is 10 GPa (20).

The wear results at the end of 300 wear iterations are shown in Figure 7.b. The model predicts, even when the tape is not wrapped in this region, a higher wear amount due to a combination of the suction effect and softer materials. This result is consistent with the experimentally observed result shown in Figure 2.b. The model predicts a lower wear on the trailing edge which can be due to inadequeate wear coefficient values for the thin-film region. The discontinuity in wear shown in Figure 7.b disappears at later iterations.

The Bidirectional Flat Tape Head

The simplest way to obtain a bidirectional version of the flat-head is to wrap the tape on both sides of the row-bar. The "soft" thin-film layer can be protected by a cap-bar as shown in Figure 8. We studied this bidirectional head in numerical wear tests similar to the unidirectional head; we varied the wrap angle $1 - 4^o$ at 2 m/s and under $T_x = 86.96$ N/m. The asperity engagement height was $\sigma_t = 36$ nm instead of 48 nm in the previous numerical tests. In order to properly simulate the bidirectionality of the head the tape speed was switched between -2 and 2 m/s at each iteration.

The results of 2° wrap after 300 wear iterations are given in Figure 9. In part (a) of this figure we see that two "expansion-regions" occur on the two edges of the head. The suction effect is similar to the unidirectional head. However, on the downstream side of the interface the constant-spacing region expands into the downstream-side-expansion-region causing the air pressure to dip below its value in the constant-spacing-region. See the air pressure profile in Figure 9.b. The contact pressure is nearly uniform in the middle section of the head and it balances the air suction. On the edges, there are the usual high pressure spikes which balance the subambient air pressure of the expansion-region, and the tape tension.

The numerical experiments showed that wear depths on the two edges of the bidirectional head are identical to the wear depth at the leading edge of the unidirectional row-bar. This result is to be expected since the contact pressure magnitude depends on the suction whose conditions are determined upstream of the flow.

The Influence of Wrap Angle on Pole-Tip Wear

The depth of gap of thin-film heads is approximately 2 μm. These heads typically tolerate

less than 1 μm of wear. Moreover, pole-tip and shield recession can cause additional spacing loss. Therefore, the prediction of the wear amounts at the pole-tip region is crucial. We simulated the long term effect of wear on head wear and pole-tip recession using the data given in Table 3.

The head wear for 10,000 iterations is plotted for three different bidirectional wrap angles in Figure 10.a. This figure shows that wear-vs-sliding distance (wear iterations) curve is initially non-linear however as a wear equilibrium is reached the curve becomes linear. Based on these curves it can be said that 1 μm wear will be reached in 8235 hours for 0.25^o wrap, 6113 hours for 0.5^o wrap and 2344 hours for 2° wrap.

Figure 10.b shows the recession of the pole tip region at the end of 10,000 wear iterations. The shallowest wrap angle 0.5^o produces the lowest pole-tip recession $\sim$ 5 nm, whereas the 2° wrap produces $\sim$ 15 nm of pole-tip recession. As the wear progresses linearly, as shown in Figure 10.a, we expect that the pole tip-recession would stay constant.

The Treshold of Wear

Our experimental work indicates, that head wear predictions given above are overestimated. In approximately 58,000 km of running in contact, during the experiment, we saw no evidence of wear on Altic in the constant gap region. More than several nanometers of wear would have resulted in change of the MR head resistance. Therefore, this suggests that wear of Altic is negligable at the contact pressures that were applied ($\sim$ 14 kPa) in the constant-spacing region. We also have seen that only 300 wear iterations ($\sim$36 km of simulation) were sufficient to predict the experimentally observed wear on the leading edge. Looking at the contact pressure levels for this case from Figure 3 we see that the highest contact pressure is $\sim$ 350 kPa. This suggests that the wear may stop

even at higher contact pressures. More controlled experiments are necessary to obtain the wear behaviour at low contact pressures.

SUMMARY AND CONCLUSIONS

We analyzed the mechanics of a moving flexible tape when it is wrapped over a flat head with small wrap angles. We showed that the problem becomes a self-acting subambient foil bearing problem where the air suction pulls the tape into contact with the head. We have seen that the upstream and downstream edges of the head have most of the wear. The worn bevel angle is less than the wrap angle (the bevel angle to wrap angle ratio is approximately 1/6 for the conditions we studied). The model agrees well with the wear contours measured with the stylus profilometer on the leading and trailing edges. The model also predicts that air suction increases with increasing wrap angle, faster tape speed and higher tape tension. The bidirectional version of the flat-head works with the same principle. We showed that, in this case, low wrap angle is desirable for reducing the head wear and the pole tip recession.

Our results suggest there is a contact pressure below which wear stops. This threshold value can be as high as few hundred kPa's for Altic assuming that the published data is applicable to our situation. However, at this point we can not exclude the possibility that there is no threshold of wear. In such a case the wear coefficient consistent with linear wear would be ~ 3 orders of magnitude smaller than what we used in this study.

REFERENCES

(1) Bhushan, B., <u>Tribology and Mechanics of Magnetic Storage Devices</u>, Springer-Verlag, New

York, NY, (1990), p. 446.

(2) Bhushan, B., Gupta, B.K., Sundaram, R., Dey, S., Anders, S. Anders, A., Brown, I.G. "Development of Hard Carbon Coatings for Thin-Film Tape Heads," <u>IEEE Trans. Mag.</u> <u>31</u>, 6, pp. 2976-2978, (1995).

(3) Bhushan, B., Lowry, J.A. "Friction and wear studies of various head materials and magnetic tapes in a linear mode accelerated test using a new nano-scratch wear measurement technique," <u>Wear</u>, <u>190</u>, pp. 1-15, (1995).

(4) Kawakubo, Y., Yahisa, Y., "Transparent Pin Wear Test on Thin-Film Magnetic Disk," <u>Journal of Tribology, Trans. ASME</u>, <u>117</u>, pp. 297-301, (1995).

(5) Bhushan, B., ed. <u>Handbook of Micro/Nano Tribology</u>, CRC Press, Boca Raton, FL, (1995), pp. 321-504.

(6) Hinteregger, H.F., Müftü, S., "Contact Tape Recording with a Flat Head Contour," <u>IEEE Trans. Mag.,</u> accepted for publication in the Intermag issue, (1996).

(7) Müftü, S., Hinteregger, H.F., "Flat Heads for High-Speed, Contact Tape Recording: Experimental Evaluation and Theoretical Analysis," to appear in the <u>Proceedings ISPS-Vol. 2, ASME,</u> Bhushan, B., Adams, G.G., Wickert, J., Connolly, D., eds., (1996).

(8) Lacey, C.A., Talke, F.E., "Measurement and Simulation of Partial Contact at the head/Tape Interface," <u>Journal of Tribology, Trans. ASME</u>, <u>114</u>, 4, pp. 646-652, (1992).

(9) Lacey, C.A., Talke, F.E., "Simulation of Wear of Tape Head Contours", <u>IEEE Trans. Mag.,</u> <u>28</u>, 5, 2554-2556, (1992).

(10) Müftü, S., Benson, R.C., "A study of the Cross-Width Variations in the Two Dimensional Foil Bearing Problem," Journal of Tribology, Trans. ASME, 118, 2, pp. 407-414, (1996).

(11) Wu, Y., Talke, F.E., "The Effect of Surface Roughness on the Head Tape Interface," Journal of Tribology, Trans. ASME, 118, 2, pp. 376-381, (1995).

(12) Hinteregger, H.F., Rogers, A.E.E., Cappallo, R.J., Webber, J.C., Petrachenko, W.T., Allen, H., "A High Data Rate Recorder for Astronomy," IEEE Trans. Mag. 27, 3, pp. 3455-3465, (1991).

(13) Müftü, S., Benson, R.C., "Modelling the Transport of Paper Webs Including Paper Permeability Effects," in Proceedings ISPS-Vol. 1, AISS, ASME, Adams, G.G., Bhushan, B., Miu, D., and Wickert, J., ed. (1995), pp. 247-258.

(14) Burgdorfer, A., The Influence of Molecular Mean Free Path on the Performance of Hydrodynamic Gas Lubricated Bearings, Journal of Basic Engineering, Trans. ASME, pp. 94-100, March, (1959).

(15) Kikuchi, N., Oden, J.T., Contact Problems in Elasticity, SIAM, Philadelphia, PA, (1988), pp. 241-266.

(16) Patton, S.T., Bhushan, B., "Friction and Wear of Metal Particle, Barium Ferrite and Metal Evaporated Tapes in Rotary Head Recorders", Journal of Tribology, Trans. ASME, 118, pp. 21-32 (1996).

(17) Gross, W.A. Fluid Film Lubrication, John Wiley & Sons, New York, NY, (1980), pp 482-549.

(18) White, J.W., "Flying Characteristics of the "Zero-Load" Slider Bearing," <u>Journal of Tribology, Trans. ASME</u>, <u>105</u>, 3, pp. 484-490, (1985).

(19) Brewen, A.T., Benson, R.C., Piarulli, V.J., "A Simple Porcedure for Determining Elsatohydrodynamic Equilibrium and Stability of a Flexible Tape Flying Over a Recording Head," <u>ASLE, SP-19</u>, Oct., (1985), pp. 43-51.

(20) Ross, C.A., and Barrese, J.J., "Mechanical Properties of Alumina Films Sputtered Over Steps," in <u>Mat. Res. Soc. Symp. Proc.</u>, Baker, S.P., Ross, C.A., Townsend, P.H., Volkert, C.A., and Borgesen, P. ed., <u>356</u>, (1995), pp. 201-207.

FIGURE CAPTIONS

Figure 1. Schematic picture of the experimental setup for the unidirectional wrap geometry.

Figure 2. The leading and trailing edge wear on the contact surface measured with a mechanical surface profiler for the wrap geometry shown in Figure 1, after 2000+ hours of running in contact. The vertical axis is presented in kAngstrom's and the horizontal axis in μm's.

Figure 3. Comparison of the experimentally measured and calculated wear profiles at the leading edge.

Figure 4. The air pressure is affected by the head-tape spacing and its interaction with the air flow components. The Couette flow brings most of the air into the interface and Poisseuille flow is responsible for pressure changes. This figure is calculated for 2.2^o unidirectional wrap, 8 m/s tape speed and 86.96 N/m tape tension.

Figure 5. The effect of a) tape speed and b) tension on the tape-gap separation for the unidirectional contour shown in Figure 1. Asperity contact starts when $h \leq 48$ nm.

Figure 6. (a) The tape displacement, and the worn head contour near the leading edge after 300 wear iterations for two different wrap angles. (b) The suction generated due to expansion of air into the "expansion-region". $V_x = 8$ m/s, $T_x = 86.96$ N/m, unidirectional wrap.

Figure 7. The leading and trailing edge wear contours after 300 wear iterations for unidirectional wrap. $V_x = 8$ m/s, $T_x = 86.96$ N/m.

Figure 8. A schematic representation of the bidirectional geometry tested numerically for stability and wear.

Figure 9. (a) The tape displacement, worn head shape, and (b) the air and contact pressures after 300 wear iterations for the <u>bidirectional</u> flat head. $V_x = 2$ m/s, $T_x = 86.96$ N/m, 2° wrap angle.

Figure 10. Each iteration corresponds to 121 m of tape running over the head. <u>Bidirectional</u> head with 2° of wrap on both sides, $V_x = 2$ m/s, $T_x = 86.96$ N/m.

E	4 GPa	σ_t	48, 36 nm
ν	0.3	P_{max}	9-10 MPa
ρ_a	1400 kgm^{-3}		
c	15.2, 27 μm		
P_a	101.3 kPa	C_r (relax.)	0.8-1
λ_a	63.5 nm	Δx	4.176 μm
μ	1.85$\times 10^{-5}$ Nsm^{-2}		

Table 1: Parameters used in numerical calculations.

Wrap Angle [^{o}]	Wear Angle [^{o}]	Maximum Suction, p/P_a	Const. Gap Suction, p/P_a
0.5	0.08	-0.18	-0.06
1.0	0.15	-0.34	-0.09
2.0	0.32	-0.56	-0.14
3.0	0.49	-0.70	-0.17
4.0	0.67	-0.76	-0.18

Table 2: Approximate wear angle of the leading edge bevel and the air suction values as a function of the wrap angle for unidirectional wrap.

Material	H [GPa]	k ($\times 10^{-9}$)	C ($\times 10^{-15}$) [m/Pa]
Al$_2$O$_3$-TiC	23.0	190[1]	1.0
Pl. Sprayed Al$_2$O$_3$	20.0[3]	558[2]	3.3
Mn-Zn-Ferrite	6.2	335[2]	6.6

[1] Tape Modeled: CrO$_2$. Contact Pressure: 105 kPa. Sliding Dist: 1 km. (3)

[2] Tape Modeled: Mag. tape w/ γ-Fe$_2$O$_3$. Contact Pressure: 25.2 kPa. Sliding Dist: 293 km, (p. 446, 1).

[3] (p. 800, 1)

Table 3: The wear constants used for the gap wear calculations ($L = 121$ m)
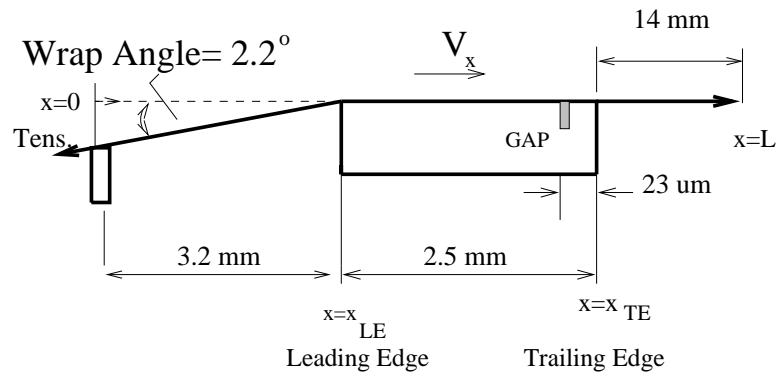
Figure 1: Schematic picture of the experimental setup for the unidirectional wrap geometry.

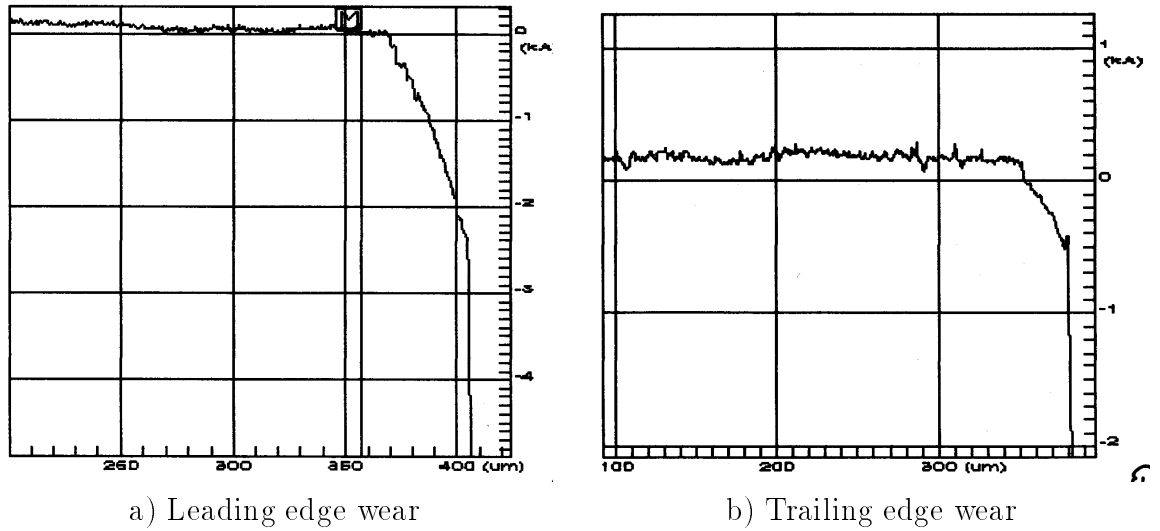a) Leading edge wear   b) Trailing edge wear

Figure 2: The leading and trailing edge wear on the contact surface measured with a mechanical surface profiler for the wrap geometry shown in Figure 1, after 2000+ hours of running in contact. The vertical axis is presented in kAngstrom's and the horizontal axis in μm's.

Figure 3: Comparison of the experimentally measured and calculated wear profiles at the leading edge.

a) The air pressure and head-tape spacing.

b) The flow components at the steady state.

Figure 4: The air pressure is affected by the head-tape spacing and its interaction with the air flow components. The Couette flow brings most of the air into the interface and Poisseuille flow is responsible for pressure changes. This figure is calculated for 2.2^o <u>unidirectional</u> wrap, 8 m/s tape speed and 86.96 N/m tape tension.

a) Tape speed variation ($T_x = 86.96 N/m$).

b) Tape tension variation ($V_x = 8m/s$).

Figure 5: The effect of a) tape speed and b) tension on the tape-gap separation for the <u>unidirectional</u> contour shown in Figure 1. Asperity contact starts when $h \leq 48$ nm.
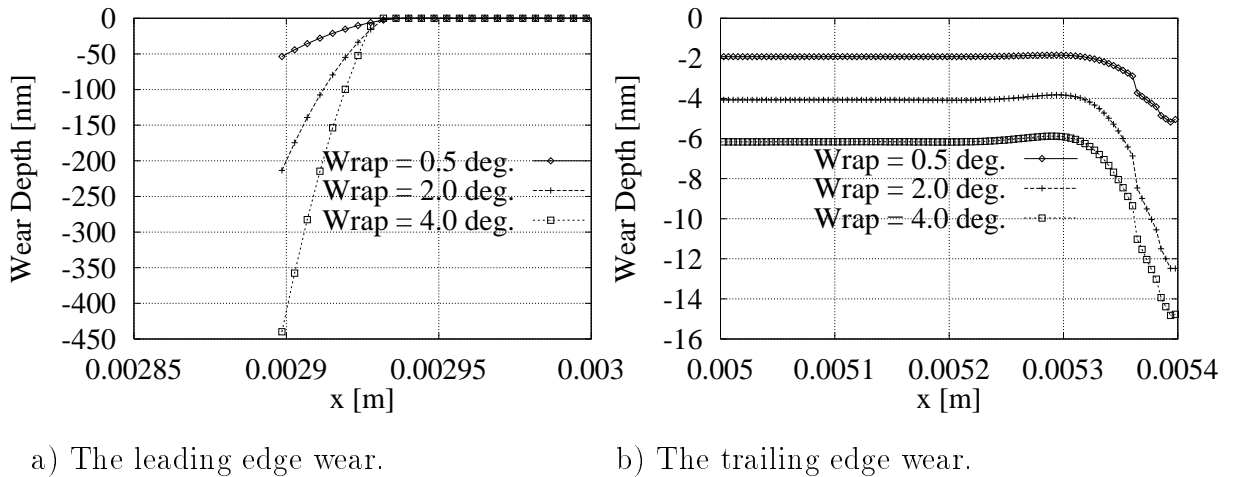
a)

b)

Figure 6: (a) The tape displacement, and the worn head contour near the leading edge after 300 wear iterations for two different wrap angles. (b) The suction generated due to expansion of air into the "expansion-region". $V_x = 8$ m/s, $T_x = 86.96$ N/m, unidirectional wrap.

a) The leading edge wear.

b) The trailing edge wear.

Figure 7: The leading and trailing edge wear contours after 300 wear iterations for unidirectional wrap. $V_x = 8$ m/s, $T_x = 86.96$ N/m.
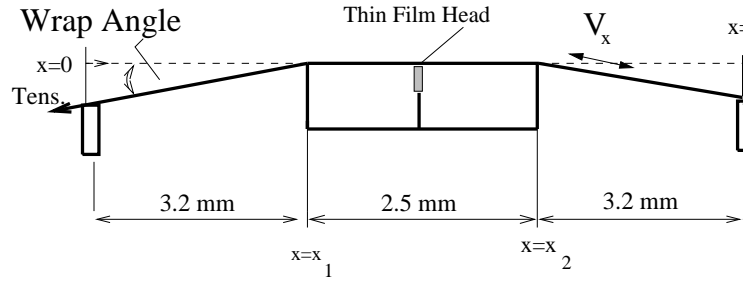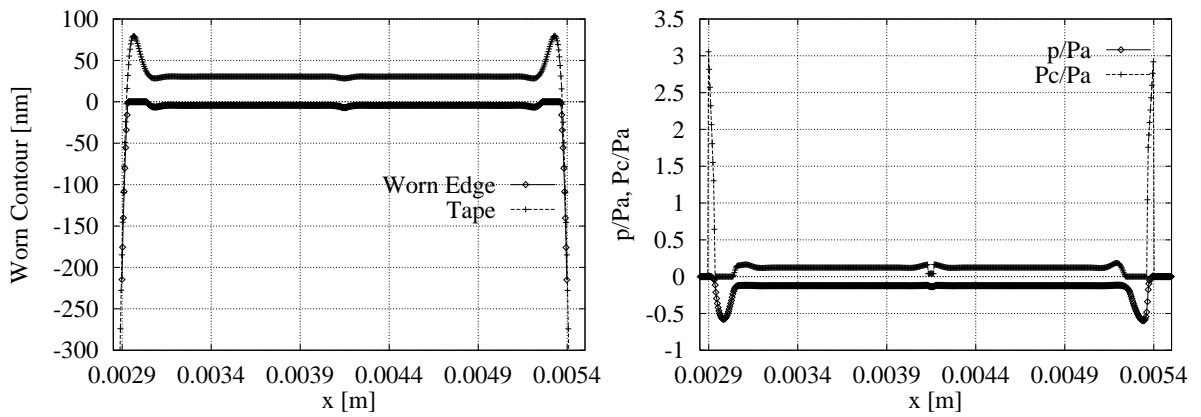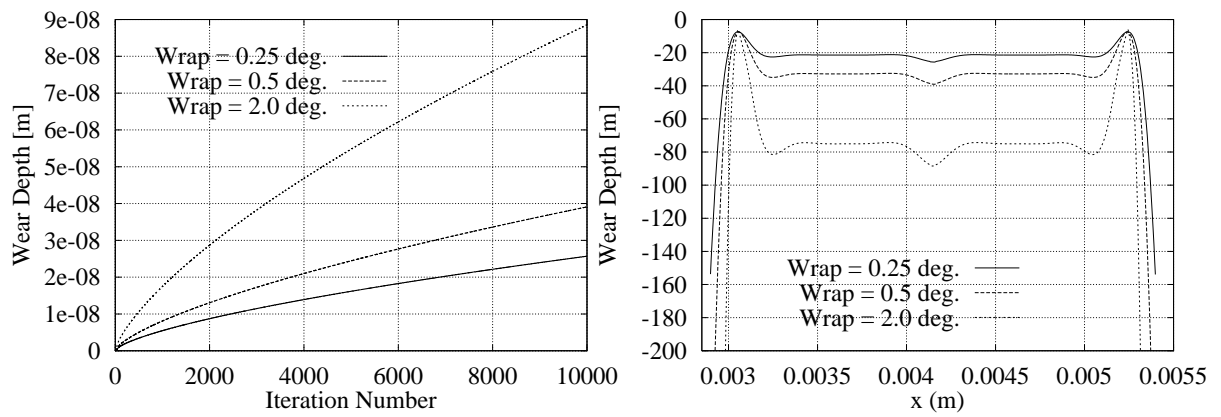
Figure 8: A schematic representation of the bidirectional geometry tested numerically for stability and wear.

a) The tape displacement and worn head contour.

b) The air and contact pressures.

Figure 9: (a) The tape displacement, worn head shape, and (b) the air and contact pressures after 300 wear iterations for the underlined bidirectional flat head. $V_x = 2$ m/s, $T_x = 86.96$ N/m, 2° wrap angle.

a) Calculated gap wear vs. wear iterations b) Worn head (end of 10,000th iteration)

Figure 10: Each iteration corresponds to 121 m of tape running over the head. <u>bidirectional</u> head with 2° of wrap on both sides, $V_x = 2$ m/s, $T_x = 86.96$ N/m.